

# Boundary conditions for fluids with internal orientational degrees of freedom: Apparent velocity slip associated with the molecular alignment

Sebastian Heidenreich,<sup>1,\*</sup> Patrick Ilg,<sup>2</sup> and Siegfried Hess<sup>1</sup>

<sup>1</sup>*Institute for Theoretical Physics, Technische Universität of Berlin, Hardenbergstrasse 36, D-10623, Germany*

<sup>2</sup>*Polymer Physics, ETH Zürich, Wolfgang-Pauli-Strasse 10, 8093 Zürich, Switzerland*

(Received 26 January 2007; published 5 June 2007)

Boundary effects are investigated for fluids with internal orientational degrees of freedom such as molecular liquids, thermotropic and lyotropic liquid crystals, and polymeric fluids. The orientational degrees of freedom are described by the second rank alignment tensor which is related to the birefringence. We use a standard model to describe the orientational dynamics in the presence of flow, the momentum balance equations, and a constitutive law for the pressure tensor to describe our system. In the spirit of irreversible thermodynamics, boundary conditions are formulated for the mechanical slip velocity and the flux of the alignment. They are set up such that the entropy production at the wall inferred from the entropy flux is positive definite. Even in the absence of a true mechanical slip, the coupling between orientation and flow leads to flow profiles with an apparent slip. This has consequences for the macroscopically measurable effective velocity. In analytical investigations, we consider the simplified case of an isotropic fluid in the Newtonian and stationary flow regime. For special geometries such as plane and cylindrical Couette flow, plane Poiseuille flow, and a flow down an inclined plane, we demonstrate explicitly how the boundary conditions lead to an apparent slip. Furthermore, we discuss the dependence of the effective viscosity and of the effective slip length on the model parameters.

DOI: [10.1103/PhysRevE.75.066302](https://doi.org/10.1103/PhysRevE.75.066302)

PACS number(s): 47.61.-k, 61.30.Vx, 67.40.Fd, 67.55.Fa

## I. INTRODUCTION

The equations of thermohydrodynamics, based on the local conservation laws and on simple constitutive relations for the heat flux and the viscous pressure tensor must be supplemented by boundary conditions. Temperature jump and velocity slip boundary conditions have been proposed over a century ago in order to describe boundary and surface effects in *rarefied gases* [1] where the mean free path  $\ell$  of the molecules can become comparable with the relevant macroscopic lengths. For dense fluids, similar effects have to be taken into consideration in microfluidics and nanorheology [2–6] where the size of the molecules is no longer extremely small compared with macroscopic length scales. Especially, the apparent slip caused by the molecular interaction with the solid surface was the reason for many theoretical and experimental studies, see for example, [7–12]. For fluids composed of particles with orientational degrees of freedom, additional constitutive equations govern the dynamics of the molecular alignment and again, boundary conditions are needed for spatially inhomogeneous situations.

In this paper, boundary conditions are formulated for the second rank alignment tensor describing the orientation of molecular liquids and nematic liquid crystals and for the velocity slip. The guiding principle, in the spirit of irreversible thermodynamics, is the same as that originally suggested for gases [13] viz.: (i) the entropy production at an interface is inferred from the entropy flux in the bulk fluid, (ii) the boundary conditions are set up such that the interfacial en-

tropy production is positive definite. The extension to molecular gas and to molecular liquids was presented in [14,15]. For a special case meant for isothermal flow of molecular liquids, polymeric melts, and nematic liquid crystals in the isotropic phase, it is demonstrated that the coupling between the alignment tensor and the friction pressure tensor which underlies the flow birefringence and shear-thinning leads to an apparent velocity slip even when the velocity obeys a stick boundary condition. The velocity and alignment profiles, as well as the effective viscosities are calculated for plane and cylindrical Couette and plane Poiseuille flow, as well as the flow down an inclined plane. The dependence of these quantities and of the apparent slip velocity on a microscopic length parameter and on the ratio between the first and second Newtonian viscosities are discussed. In experiments slip lengths and the viscosities of thin films of Newtonian liquids were measured and studied by Jacobs *et al.* [16]. Furthermore, a recent thermodynamic formulation of boundary conditions building upon the pioneering work of Waldmann [13] was derived in [17–19].

This paper proceeds as follows. First, the relaxation equation for the alignment tensor in spatially inhomogeneous systems is introduced and the constitutive equation for the pressure tensor are presented in Secs. II A and II B, respectively. In Sec. III, we show how the entropy production at the interface can be used to impose boundary conditions. The model equations, the constitutive equations for the pressure tensor and the momentum balance give us a closed set of equations. In Sec. IV we consider the isotropic phase where terms nonlinear in the alignment tensor and in the velocity gradient are disregarded. In the following sections we discuss different flow geometries as already mentioned.

---

\*Corresponding author. Electronic address: [sebastian@itp.physik.tu-berlin.de](mailto:sebastian@itp.physik.tu-berlin.de)

## II. THE MODEL EQUATIONS FOR A SPATIALLY INHOMOGENEOUS FLUID

### A. Relaxation equation for the alignment tensor

The alignment of the effectively uniaxial particles with a molecular axis parallel to the unit vector  $\mathbf{u}$  is characterized by an orientational distribution function  $f(\mathbf{u}, t)$ . The appropriate order parameter for a liquid crystal in its isotropic and nematic phases is the second rank alignment tensor

$$\mathbf{a} = \sqrt{\frac{15}{2}} \langle \overline{\mathbf{u}\mathbf{u}} \rangle \equiv \int f(\mathbf{u}, t) \sqrt{\frac{15}{2}} \overline{\mathbf{u}\mathbf{u}} d^2u, \quad (1)$$

which is an anisotropic second moment characterizing the distribution. The symbol  $\overline{\mathbf{x}}$  indicates the symmetric traceless part of a tensor  $\mathbf{x}$ , i.e., with Cartesian components denoted by greek subscripts, one has  $\overline{x_{\mu\nu}} = (1/2)(x_{\mu\nu} + x_{\nu\mu}) - (1/3)x_{\lambda\lambda}\delta_{\mu\nu}$ . Frequently, the alignment tensor is also referred to as  $\mathbf{Q}$ -tensor, sometimes as  $\mathbf{S}$ -tensor.

The symmetric traceless part  $\overline{\boldsymbol{\epsilon}}$  of the dielectric tensor  $\boldsymbol{\epsilon}$  which gives rise to birefringence is proportional to the alignment tensors, viz.  $\overline{\boldsymbol{\epsilon}} = \varepsilon_a \mathbf{a}$ , with characteristic coefficient  $\varepsilon_a$  specifying the optical anisotropy. The shear flow induced modifications of the alignment can be detected optically [20].

For the special case of uniaxial symmetry (uniaxial phase) the alignment tensor  $\mathbf{a}$  can be parametrized by a scalar order parameter  $a$  and the director  $\mathbf{n}$ , i.e.,  $\mathbf{a} = a(3/2)^{1/2} \overline{\mathbf{n}\mathbf{n}}$ , such that  $a^2 = \mathbf{a} : \mathbf{a}$ , and  $-\sqrt{5}/2 \leq a = (3/2)^{1/2} \mathbf{a} : \overline{\mathbf{n}\mathbf{n}} \leq \sqrt{5}$ . The parameter  $a$  is therefore proportional to the Maier-Saupe order parameter  $S_2 \equiv \langle P_2(\mathbf{u} \cdot \mathbf{n}) \rangle = a/\sqrt{5}$ , where  $P_2$  denotes the second Legendre polynomial. Clearly, by definition, the order parameter  $a$  is bounded, just as  $S_2$ .

The nonlinear relaxation equation for the alignment tensor  $\mathbf{a}$ , coupled to the velocity gradient field and an expression for the contribution to the pressure or stress tensor associated with the alignment were derived in [21,22]. The generalization to a spatially inhomogeneous situation was presented in [23], see also [24] for related works.

The equations involve characteristic phenomenological coefficients viz. the relaxation time coefficient  $\tau_a > 0$ , as well as  $\tau_{ap}$  which determine the strength of the coupling between the alignment and the pressure tensor or the velocity gradient, dimensionless coefficient  $\kappa$ , and parameters for the Landau-de Gennes potential to be discussed later. These parameters are linked with the pseudocritical temperature  $T^*$ , the nematic-isotropic transition temperature  $T_K$  with  $T_K > T^*$ , and with the value of the alignment just below  $T_K$ .

The equation of change for the alignment tensor  $\mathbf{a}$ , in the presence of a flow field  $\mathbf{v}$  reads [21,22]:

$$\frac{d\mathbf{a}}{dt} - 2\overline{\boldsymbol{\Omega} \times \mathbf{a}} - 2\kappa \overline{\boldsymbol{\Gamma} \cdot \mathbf{a}} + \nabla \cdot \mathbf{b} + \tau_a^{-1} \Phi^a(\mathbf{a}) = -\sqrt{2} \frac{\tau_{ap}}{\tau_a} \boldsymbol{\Gamma}. \quad (2)$$

The symmetric traceless tensor

$$\Phi^a(\mathbf{a}) = \partial\Phi/\partial\mathbf{a} - \nabla \cdot [\partial\Phi/\partial(\nabla\mathbf{a})] \quad (3)$$

is the derivative of the potential function  $\Phi$ , to be specified later, with respect to the alignment tensor and its spatial derivative. The symbol  $\frac{d\cdots}{dt}$  stands for the substantial time derivative  $\frac{\partial\cdots}{\partial t} + \mathbf{v} \cdot \nabla \cdots$ . The variables  $\boldsymbol{\Gamma}$  and  $\boldsymbol{\Omega}$  denote the symmetric traceless part of the velocity gradient tensor (strain rate tensor)  $\boldsymbol{\Gamma} \equiv \overline{\nabla\mathbf{v}}$ , and the vorticity  $\boldsymbol{\Omega} \equiv (\nabla \times \mathbf{v})/2$ , respectively. In the case of a simple shear flow  $\mathbf{v} = \dot{\gamma}y\mathbf{e}^x$  in the  $x$  direction, gradient in the  $y$  direction, and vorticity in the  $z$  direction, to be considered later, these quantities simplify to  $\boldsymbol{\Gamma} = \dot{\gamma}\mathbf{e}^x\mathbf{e}^y$  and  $\boldsymbol{\Omega} = -(1/2)\dot{\gamma}\mathbf{e}^z$ . The unit vectors parallel to the coordinate axes are denoted by  $\mathbf{e}^x, \mathbf{e}^y, \mathbf{e}^z$ .

In Refs. [22,25] the symbol  $\sigma$  was used instead of  $\kappa$ . The special values 0 and  $\pm 1$  for the coefficient  $\kappa$  in (2) correspond to corotational and codeformational time derivatives. From the solution of the generalized Fokker-Planck equation one finds, for long particles,  $\kappa \approx 3/7 \approx 0.4$ .

In a spatially inhomogeneous system, the (third rank) alignment flux tensor  $\mathbf{b} \sim \langle \mathbf{c}\mathbf{u}\mathbf{u} \rangle$ , where  $\mathbf{c}$  is a peculiar molecular velocity, must be taken into account. Following the arguments given in [23], the constitutive relation

$$\mathbf{b} = -D_a \nabla \Phi^a \quad (4)$$

is used with the alignment diffusion coefficient  $D_a$ . This isotropic approximation is used for simplicity. It is valid when the three diffusion coefficients linking the vector, second and third rank irreducible tensor parts of  $\mathbf{b}$  with those of  $\nabla\Phi^a$  are practically equal. For an experimental situation where the anisotropy of an alignment tensor diffusion matters cf. [26]. According to the general principles of irreversible thermodynamics, a coupling of the vector part of  $\mathbf{b}$  with the heat flux vector exists. This is akin to the coupling between the Kagan vector and the heat flux considered in the kinetic theory of molecular gases [1,27]. Here such an effect is disregarded.

### B. Constitutive relation for the pressure tensor

The alignment is not only influenced by the flow but the flow properties as characterized by the friction pressure tensor are affected by the alignment. The full pressure tensor  $\mathbf{P}$  consists of a hydrostatic pressure  $p$ , an antisymmetric part, and the symmetric traceless part  $\overline{\mathbf{p}}$  frequently referred to as friction pressure tensor [21]. In Cartesian tensor notation (greek subscripts indicate the components 1, 2, 3 pertaining to  $x, y, z$  directions, the summation convention is used) the pressure tensor  $P_{\nu\mu}$  occurring in the momentum balance equation (no external field,  $\rho$  is the mass density)

$$\rho \frac{dv_\mu}{dt} + \nabla_\nu P_{\nu\mu} = 0 \quad (5)$$

is decomposed according to

$$P_{\nu\mu} = P\delta_{\nu\mu} + \frac{1}{2}\varepsilon_{\nu\mu\lambda}p_\lambda + \overline{p}_{\nu\mu}. \quad (6)$$

Here  $P = \frac{1}{3}P_{\lambda\lambda}$  is the trace part,  $\overline{p_{\mu\nu}} = \frac{1}{2}(P_{\mu\nu} + P_{\nu\mu}) - \frac{1}{3}P_{\lambda\lambda}\delta_{\mu\nu}$  is the symmetric traceless part of the tensor, and  $p_\lambda = \varepsilon_{\lambda\nu\mu}P_{\nu\mu}$  is the component of the pseudovector associated with the antisymmetric part of the pressure tensor.

In the following, the trace part  $P$  is identified with the hydrostatic pressure linked with the local density and temperature by the equilibrium equation of state. The symmetric traceless friction pressure tensor consists of an isotropic contribution as already present in fluids composed of spherical particles or in fluids of nonspherical particles in a perfectly isotropic state with zero alignment, and a part explicitly depending on the alignment tensor

$$\overline{\mathbf{p}} = -2\eta_{\text{iso}}\mathbf{\Gamma} + \overline{\mathbf{p}}_{\text{al}}, \quad (7)$$

with [22]

$$\overline{\mathbf{p}}_{\text{al}} = \frac{\rho}{m}k_B T \left( \sqrt{2} \frac{\tau_{ap}}{\tau_a} \mathbf{\Phi}^a - 2\kappa \mathbf{a} \cdot \mathbf{\Phi}^a \right). \quad (8)$$

Here  $m$  and  $\rho$  are the mass of a particle and the mass density,  $\rho/m$  is the number density, and  $p_{\text{kin}} = \frac{\rho}{m}k_B T$  is the equilibrium kinetic pressure which is used as reference value for pressures. In equilibrium one has  $\mathbf{\Phi}(\mathbf{a}) = \mathbf{0}$  and consequently  $\overline{\mathbf{p}}_{\text{al}} = \mathbf{0}$ . The occurrence of the same coupling coefficients  $\tau_{ap}$  in (8) as in (2) is due to Onsager symmetry relations. For studies on the rheological properties in the isotropic and in the nematic phases with stationary flow alignment, following from (2) and (8) see [21–23,28].

The vector associated with antisymmetric part of the pressure tensor appears in the conservation law of the angular momentum. It vanishes identically for fluids of particles without rotational degrees of freedom. In the absence of torques due to external orienting fields the antisymmetric part of the pressure tensor also vanishes provided that average rotational velocity of the particles relaxes to the local vorticity within a time which is short compared with the relaxation time for reorientation which is determined by  $\tau_a$ . Implicitly, this assumption has already been made in (2). In the same approximation, the pseudovector linked with the antisymmetric part of the friction pressure tensor is given by

$$p_\mu = -2 \frac{\rho}{m} k_B T \varepsilon_{\mu\nu\lambda} a_{\nu\kappa} \Phi_{\kappa\lambda}^a. \quad (9)$$

Thus the constitutive law for  $\Phi_{\mu\nu}$  will also provide an expression for the antisymmetric part of the pressure tensor [29]. In the nematic phase, e.g., the relation  $p_\mu = 0$ , with (2) and (9) yields the flow alignment angle.

### C. Landau-de Gennes potential

In previous studies the (dimensionless) Landau-de Gennes potential  $\Phi = \Phi(\mathbf{a})$ , viz.,

$$\Phi^{\text{LG}} = (1/2)A(T)\mathbf{a}:\mathbf{a} - (1/3)\sqrt{6}B(\mathbf{a} \cdot \mathbf{a}):\mathbf{a} + (1/4)C(\mathbf{a}:\mathbf{a})^2 \quad (10)$$

has been used with  $A(T) = A_0(1 - T^*/T)$ . Here  $A_0, B, C$  [with  $C < 2B^2/(9A_0)$ ] are positive dimensionless coefficients. The characteristic temperature  $T^*$  is also a model parameter. The value of  $A_0$  depends on the proportionality coefficient chosen between  $\mathbf{a}$  and  $\langle \overline{\mathbf{u}\mathbf{u}} \rangle$ . The choice made above implies  $A_0 = 1$ , cf. [21]. The coefficients, on the one hand, are linked with measurable quantities and, on the other hand, can be related to molecular quantities within the framework of a mesoscopic theory [30–32]. For lyotropic liquid crystals the con-

In a spatially inhomogeneous situation, the potential function also contains a contribution  $\Phi^{\text{inh}}$  involving the spatial derivative  $\nabla \mathbf{a}$  of the alignment tensor. Again for simplicity, the isotropic case is considered which implies that, in the nematic phase, all three Frank elasticity coefficients are equal. Thus one has, in component notation,

$$\Phi^{\text{inh}} = (1/2)\xi_0^2 (\nabla_\lambda a_{\mu\nu}) (\nabla_\lambda a_{\mu\nu}), \quad (11)$$

with a characteristic length  $\xi_0$ . Clearly, the value of the total potential  $\Phi = \Phi^{\text{LG}} + \Phi^{\text{inh}}$  is higher in a spatially inhomogeneous system as compared with a homogeneous one. With this particular choice, the derivative of the potential occurring in the relaxation equation (2) becomes

$$\mathbf{\Phi}^a(\mathbf{a}) = A\mathbf{a} + \dots - \xi_0^2 \Delta \mathbf{a}, \quad (12)$$

the ellipses stand for terms nonlinear in  $\mathbf{a}$ . These may be disregarded in the isotropic phase.

### III. BOUNDARY CONDITIONS

In the spirit of irreversible thermodynamics, Waldmann [13] suggested to set up boundary conditions such that the interfacial entropy production is positive definite. For a fluid in contact with a solid wall moving with the velocity  $\mathbf{v}^w$  one has [15,35]

$$\theta^w = \int df T^{-1} [k_\mu^{\text{tan}} (v_\mu - v_\mu^w)^{\text{tan}} + (\rho/m) k_B n_\lambda b_{\lambda\mu\nu} \Phi_{\mu\nu}]. \quad (13)$$

Here  $df$  is the surface element,  $\mathbf{n}$  is the outer normal of the fluid and the superscript tan indicates a tangential component which is parallel to the surface, e.g.,  $v_\mu^{\text{tan}} = v_\mu - n_\mu n_\nu v_\nu$ . Furthermore,

$$k_\mu = n_\nu (P_{\nu\mu} - P \delta_{\nu\mu}) \quad (14)$$

is the friction force density. It is tacitly assumed that  $P$  is the hydrostatic equilibrium pressure, which means that a scalar pressure associated with the bulk viscosity is disregarded or that the fluid is practically incompressible, viz.,  $\nabla \cdot \mathbf{v} = 0$ .

Just as in [15], we follow the notation which Vestner [14] used for molecular gases where the equations are linear in the alignment tensor which, in addition, has a different microscopic meaning. The boundary conditions for the velocity and the alignment tensor are

$$(v_\mu - v_\mu^w)^{\text{tan}} = C_m v_{\text{th}} p_{\text{kin}}^{-1} k_\mu^{\text{tan}} + C_{m\lambda} n_\lambda b_{\lambda\mu\nu} n_\nu, \quad (15)$$

$$\Phi_{\mu\nu}^a = C_{am} p_{\text{kin}}^{-1} \overline{k_{\mu}^{\text{tan}}} n_{\nu} + C_a v_{\text{th}}^{-1} n_{\lambda} b_{\lambda\mu\nu}. \quad (16)$$

Here the kinetic pressure  $p_{\text{kin}} = (\rho/m)k_B T$  and the thermal velocity  $v_{\text{th}} = \sqrt{k_B T/m}$  are used as reference values for the pressure and the velocity. The dimensionless coefficients  $C$  specify the boundary behavior, the subscripts  $m$  and  $a$  refer to mechanical and alignment, respectively. The diagonal coefficients are non-negative, viz.,  $C_m \geq 0$ ,  $C_a \geq 0$ . The off-diagonal ones obey the Onsager-Casimir relation  $C_{am} = -C_{ma}$ . The slip velocity is  $\delta v_{\mu} = -(v_{\mu} - v_{\mu}^{\text{slip}})^{\text{tan}}$ . For  $C_{ma} = 0$  and with  $k_{\mu} = -\eta m_{\nu} \nabla_{\nu} v_{\mu}$ , where  $\eta$  is the shear viscosity, (15) is equivalent to

$$\delta v_{\mu} = \ell_v n_{\nu} \nabla_{\nu} v_{\mu}^{\text{tan}}, \quad (17)$$

with the slip length

$$\ell_v = C_m \eta v_{\text{th}} p_{\text{kin}}^{-1} \geq 0. \quad (18)$$

In the following, it will be demonstrated that the coupling between the alignment and the flow field leads to an apparent velocity slip even when  $C_m = 0$  and consequently  $\ell_v = 0$ .

#### IV. APPARENT VELOCITY SLIP

##### A. Special case: isotropic phase, small shear rates

Next the equations for the bulk fluid and the boundary conditions are applied to special geometries where the spatial dependence is essentially one-dimensional, viz., to a plane Couette and a plane Poiseuille flow. The attention is focused on the isotropic phase where terms nonlinear in the alignment tensor can be disregarded and on the Newtonian flow regime where only terms linear in the velocity gradient are taken into account. The antisymmetric part of the pressure tensor vanishes in this case. Then, with (6), (7), and (8), the momentum balance equation (5) reduces to

$$\rho \frac{\partial v_{\mu}}{\partial t} + \nabla_{\mu} P = \eta_{\text{iso}} \Delta v_{\mu} - p_{\text{kin}} \sqrt{2} \frac{\tau_{ap}}{\tau_a} \varphi_{\mu}, \quad (19)$$

with

$$\varphi_{\mu} = \nabla_{\nu} \Phi_{\nu\mu}^a. \quad (20)$$

Similarly, the relaxation equation (2) for the alignment tensor is approximated by

$$\frac{\partial a_{\mu\nu}}{\partial t} + \tau_a^{-1} (\Phi_{\mu\nu}^a - \ell_a^2 \Delta \Phi_{\mu\nu}^a) = -\sqrt{2} \frac{\tau_{ap}}{\tau_a} \overline{\nabla_{\nu} v_{\mu}}, \quad (21)$$

and it is understood that only terms linear in the alignment tensor are considered in  $\Phi_{\mu\nu}^a$ , cf. (12). The characteristic length  $\ell_a$  associated with the alignment diffusion is defined by

$$\ell_a^2 = D_a \tau_a. \quad (22)$$

For stationary situation, application of  $\nabla_{\nu}$  on (21) leads to

$$(\varphi_{\mu} - \ell_a^2 \Delta \varphi_{\mu}) = -(1/2) \sqrt{2} \tau_{ap} \Delta v_{\mu}. \quad (23)$$

Elimination of  $\Delta \mathbf{v}$  from (23) with the help of (19), again for a steady state where the time derivatives vanish, yields

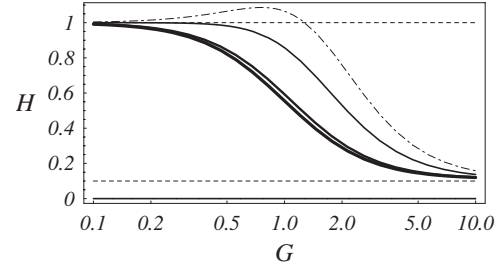


FIG. 1. Non-Newtonian viscosity for the plane Couette flow in the isotropic phase for  $Q=8$ . Here  $G = \gamma A^{-1} \tau_a$  is the shear rate and  $H$  is the viscosity in units of the first Newtonian viscosity  $\eta$ . The values for  $\kappa$  are, from left to right, 0, 0.4, 1.0, and 1.2 (dashed curve).

$$[1 + \tau_{ap}^2 / (\tau_0 \tau_a)] \varphi_{\mu} - \ell_a^2 \Delta \varphi_{\mu} = -\eta_{\text{iso}}^{-1} \tau_{ap} \nabla_{\mu} P. \quad (24)$$

The relaxation time  $\tau_0$  is related to the second Newtonian viscosity  $\eta_{\text{iso}}$  by  $\eta_{\text{iso}} = p_{\text{kin}} \tau_0$ . Similarly, the first Newtonian viscosity  $\eta$  is linked with the relaxation time  $\tau_p$  by  $\eta = p_{\text{kin}} \tau_p$ , and one has [1]  $\tau_0 / \tau_p = 1 - \tau_{ap}^2 / (\tau_a \tau_p)$ . The abbreviation

$$Q = \frac{\tau_{ap}^2}{\tau_0 \tau_a} = \frac{\tau_{ap}^2}{\tau_a \tau_p} \left(1 - \frac{\tau_{ap}^2}{\tau_a \tau_p}\right)^{-1} \geq 0, \quad (25)$$

is introduced. Notice that  $\tau_{ap}^2 / (\tau_a \tau_p) < 1$ . The quantity  $Q$  which is a measure for the strength of the coupling between the pressure tensor and the alignment is linked by the ratio  $\eta / \eta_{\text{iso}}$  between the first and second Newtonian viscosities by

$$Q = \frac{\eta}{\eta_{\text{iso}}} - 1. \quad (26)$$

Now (24) is rewritten as

$$\varphi_{\mu} - \ell^2 \Delta \varphi_{\mu} = -\eta^{-1} \tau_{ap} \nabla_{\mu} P \quad (27)$$

with the characteristic length  $\ell$  related to  $\ell_a$  by

$$\ell^2 = \ell_a^2 (1 + Q)^{-1} = \ell_a^2 \left(1 - \frac{\tau_{ap}^2}{\tau_a \tau_p}\right). \quad (28)$$

The solutions of the homogeneous part of (27) couple with the velocity field due to (23) via the boundary condition. Next, this point is discussed for a simple one-dimensional spatial dependence as encountered in plane Couette and in a plane Poiseuille flow. The parameter  $Q$  can be inferred from the nonlinear flow behavior, in particular from the non-Newtonian viscosity in the limits of small and large shear rates. The stationary solution of (2) in the isotropic phase and for a plane Couette flow where the boundary effects to be discussed below are ignored, were presented in [22]. A representative example is shown in Fig. 1. The transition from the first to the second Newtonian viscosity depends on the parameter  $\kappa$ , the limiting values determining  $Q$  are not affected by  $\kappa$ . The following calculations focus on the effect of the boundary conditions in the limiting case of small shear rates, viz. the linear flow regime.

### B. Special case: one-dimensional spatial dependence

For a flow in the  $x$  direction and its gradient in the  $y$  direction as it occurs between flat plates which are perpendicular to the  $y$  direction one has

$$\Gamma_{\nu\mu} = \overline{\nabla_\nu v_\mu} = \gamma(y) \overline{e_\nu^x e_\mu^y}, \quad (29)$$

with the shear rate  $\gamma = \gamma(y)$ , the unit vectors parallel to the coordinate axes are denoted by  $\mathbf{e}^x$ ,  $\mathbf{e}^y$ , and  $\mathbf{e}^z$ . Similarly, the ansatz

$$\Phi_{\mu\nu}^a = \sqrt{2} \alpha(y) \overline{e_\nu^x e_\mu^y}, \quad (30)$$

is made which implies  $\varphi_\mu = (1/2) \sqrt{2} \alpha'(y) e_\mu^x$ . The prime indicates the derivative with respect to  $y$ . In this special case and for stationary situation, (21) reduces to

$$\alpha - \ell_a^2 \alpha'' = -\tau_{ap} \gamma. \quad (31)$$

Similarly, (27) where the momentum balance has been taken into account, is equivalent to

$$\alpha' - \ell^2 \alpha''' = -\tau_{ap} \eta^{-1} \frac{\delta P}{L}. \quad (32)$$

For a Poiseuille flow the pressure gradient in the  $x$  direction is given by the ratio of the pressure difference  $\delta P$  and the length  $L$  of the flow device. In the case of a Couette flow one has  $\delta P = 0$ .

The boundary condition (16) for the alignment, at a wall with the outer normal in the positive  $y$  direction now reduces to

$$\alpha = -C_a v_{th}^{-1} D_a \alpha' = -c_a \ell \alpha'. \quad (33)$$

Here (4) and  $C_{am} = 0$  were used. The abbreviation

$$c_a = C_a \frac{D_a}{\ell v_{th}} = C_a \frac{\ell_a \sqrt{1+Q}}{\tau_a v_{th}} \quad (34)$$

was introduced. Next, solutions of the differential equations (31) and (32), with the appropriate boundary conditions are presented for the Couette and the Poiseuille flow geometry.

### C. Plane Couette flow

A Couette flow between (identical) plates separated by the distance  $2h$  is considered. The plates located at  $y=h$  and  $y=-h$  move with the velocities  $\mathbf{v}^w$  and  $-\mathbf{v}^w$ , respectively, in the  $x$  direction. Here one has  $\delta P = 0$  and the solution of (32), with the symmetry of the setup taken into account, is

$$\alpha = \alpha_0 + \alpha_1 \cosh(y/\ell). \quad (35)$$

Likewise, for the shear rate the ansatz

$$\gamma = \gamma_0 + \gamma_1 \cosh(y/\ell) \quad (36)$$

is made. For the  $x$  component of the velocity one has

$$v(y) = \gamma_0 y + \gamma_1 \ell \sinh(y/\ell). \quad (37)$$

The coefficients  $\alpha_0, \alpha_1, \gamma_0, \gamma_1$  must be determined with the help of (31) and of the boundary conditions.

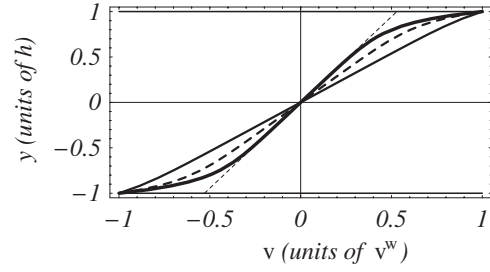


FIG. 2. The velocity vs the distance in units of  $h$  is plotted for plane Couette flow, cf. (43). The model parameters are  $Q=8$ ,  $h/\ell=9$ , and  $c_a=0$  (thick dashed line),  $c_a=1$  (thin line),  $c_a=10$  (thick line).

Now a no-slip boundary condition corresponding to  $C_m = C_{ma} = 0$  is assumed, cf. (15). This implies  $v^w = \gamma_0 h + \gamma_1 \ell \sinh(h/\ell)$ . The external shear rate  $\gamma^{\text{ext}}$  is related to  $\gamma_0, \gamma_1$  by

$$\gamma^{\text{ext}} = v^w/h = \gamma_0 + \gamma_1 (\ell/h) \sinh(h/\ell). \quad (38)$$

The boundary condition (33) for the alignment leads to

$$\alpha_0 = -\alpha_1 [\cosh(h/\ell) + c_a \sinh(h/\ell)]. \quad (39)$$

Two further relations are needed for the determination of the coefficients, viz.

$$\alpha_0 = -\tau_{ap} \gamma_0, \quad Q \alpha_1 = \tau_{ap} \gamma_1 \quad (40)$$

follow from the differential equation (31). Insertion of these relations into (39) yields

$$Q \gamma_0 = \gamma_1 [\cosh(h/\ell) + c_a \sinh(h/\ell)]. \quad (41)$$

From this relation and (38) follows

$$\gamma_0 = R \gamma^{\text{ext}}, \quad R = \left( 1 + Q \frac{\ell}{h} \frac{\tanh(h/\ell)}{1 + c_a \tanh(h/\ell)} \right)^{-1}. \quad (42)$$

The resulting solution for the velocity field is

$$v(y) = R v^w \left( \frac{y}{h} + Q \frac{\ell}{h} \frac{\sinh(y/\ell)}{\cosh(h/\ell) + c_a \sinh(h/\ell)} \right). \quad (43)$$

Likewise, for  $\alpha$  one finds

$$\alpha(y) = -\tau_{ap} R \frac{v^w}{h} \left( 1 - \frac{\cosh(y/\ell)}{\cosh(h/\ell) + c_a \sinh(h/\ell)} \right). \quad (44)$$

The velocity profile is plotted in Fig. 2 for  $Q=8$  and  $h/\ell=9$ , corresponding to  $2h/\ell_a=6$ . The velocity is presented in units of the wall velocity  $v^w$ , the  $y$  coordinate is in units of  $h$ , i.e., one-half the separation between the moving plates. The thick curve pertains to  $c_a=0$ , the other curves are for  $c_a=1$ , and  $c_a=10$  (thin curve). Linear extrapolation of the velocity in the center towards the wall at  $y=h$ , e.g., see the dashed line shown for  $c_a=0$ , yields the velocity  $h\gamma_0$  which is smaller than the wall velocity  $v^w$ . Thus one has an effective slip velocity

$$\delta v^{\text{eff}} = v^w - h\gamma_0 = (1-R)v^w = (1-R)h\gamma^{\text{ext}}. \quad (45)$$

An effective slip length  $\ell_v^{\text{eff}}$  is defined by

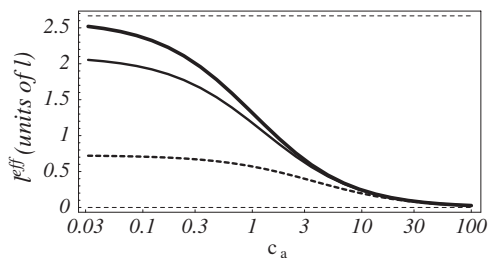


FIG. 3. The effective slip length in units of  $l$  is plotted as a function of the parameter  $c_a$  for the same conditions as in Fig. 2. The parameters are  $Q=8$ ,  $\ell=2$ , and  $h=3$  (thick dashed line),  $h=30$  (thin line),  $h=300$  (thick line).

$$\delta v^{\text{eff}} = \ell_v^{\text{eff}} \gamma^{\text{ext}}. \quad (46)$$

From the relations above follows

$$\ell_v^{\text{eff}} = \ell Q \tanh(h/\ell) \left[ 1 + \left( c_a + Q \frac{\ell}{h} \right) \tanh(h/\ell) \right]^{-1}. \quad (47)$$

For  $\ell \ll h$ , this expression reduces to

$$\ell_v^{\text{eff}} \rightarrow \frac{\ell Q}{1 + c_a + Q \frac{\ell}{h}}. \quad (48)$$

Clearly, the apparent slip is largest for  $c_a=0$ . For  $c_a \gg 1$ , on the other hand, the simple Couette flow profile is approached as Fig. 3 implies.

In Fig. 4, the effective slip length in units of  $h$  as a function of the Couette cell size  $h$  is displayed. For small ratio  $\ell^{\text{eff}}/h$ , the effective slip length has a significant effect on the flow. For higher values of the ratio the effect becomes more and more marginal. The slip effect can be disregarded for high ratio of the systems length compared to the molecular length. In the case where we define the effective velocity via an extrapolation of a small linear part of the velocity profile the slip length has in principle the same value for higher values of the ratio  $h/\ell$ . For smaller values the slip length decreases slightly depending on the parameter value of  $Q$ .

An effective viscosity can be defined via the  $yx$  component of the pressure tensor divided by the external shear rate, viz,

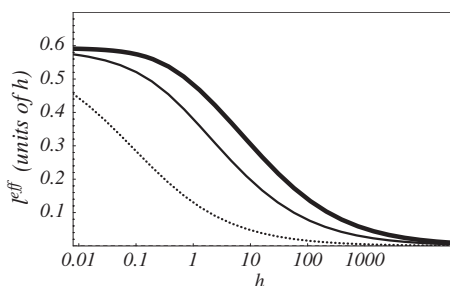


FIG. 4. The effective slip length (47) in units of  $h$  vs  $h$  is displayed for plane Couette flow. The model parameter are  $Q=8$  and  $c_a=0$  (dashed line),  $c_a=1$  (thin line),  $c_a=10$  (thick line).

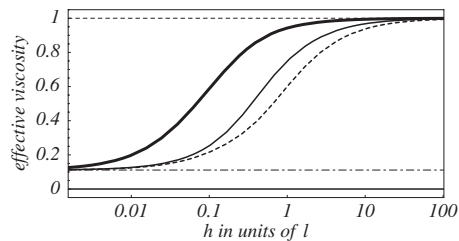


FIG. 5. The reduced effective viscosity  $\eta_{\text{eff}}/\eta$  as a function of  $h/l$  for plane Couette flow is displayed. The parameters are  $Q=2$  and  $c_a=0$  (thick dashed line),  $c_a=1$  (thin line),  $c_a=10$  (thick line).

$$\eta_{\text{eff}} = \frac{-P_{yx}}{\gamma^{\text{ext}}} = p_{\text{kin}} \left( \tau_0 \gamma(h) - \frac{\tau_{ap}}{\tau_a} \alpha(h) \right) / \gamma^{\text{ext}}. \quad (49)$$

The solutions given above for  $\gamma(y)$  and  $\alpha(y)$  eventually lead to

$$\eta_{\text{eff}} = R \eta. \quad (50)$$

In the limit  $\ell \ll h$  one has

$$\eta^{\text{eff}} \rightarrow \eta \frac{1 + c_a}{1 + c_a + Q \frac{\ell}{h}}. \quad (51)$$

For  $c_a \gg 1$ , where the simple Couette flow profile is recovered, the effective viscosity becomes equal to the shear viscosity.

In Fig. 5, the effective viscosity is plotted for  $Q=2$ ,  $\eta=1$  and several values of  $c_a=0, 1, 10$ . It can be recognized that for high values of the ratio  $h/\ell$  the effective viscosity approaches the shear viscosity  $\eta$ . But if the magnitude of  $h$  is comparable to  $\ell$ , the effective viscosity is much smaller than the shear viscosity. This effect depends strongly on the parameter  $c_a$ . For high  $c_a$ , this effect is negligible whereas for small values of  $c_a$  the shear viscosity is effected dramatically by the influence of the boundary conditions, as soon as  $Q \neq 0$ . If the first and the second non-Newtonian viscosity are equal and therefore  $Q=0$  (no coupling of the alignment on the velocity), the effective viscosity is not influenced by the boundary conditions as expected.

#### D. Plane Poiseuille flow

Consider now a flow between (identical) flat plates located at  $y=h$  and  $y=-h$ . In the Poiseuille case, the walls are at rest and the flow is driven by the constant pressure gradient  $\delta P/L$ , where  $P=P(x)$  is assumed. Notice that one has  $\delta P = P(L) - P(0) < 0$  for a flow in the  $x$  direction. Taking the symmetry of the problem into account, the ansatz

$$\alpha(y) = \alpha_2 \frac{y}{h} + \alpha_3 \sinh(y/\ell) \quad (52)$$

is now made for  $\alpha(y)$ . Similarly, for the shear rate one writes

$$\gamma(y) = \gamma_2 \frac{y}{h} + \gamma_3 \sinh(y/\ell). \quad (53)$$

With the no-slip condition  $v(h)=v(-h)=0$  taken into account, the resulting velocity field is given by

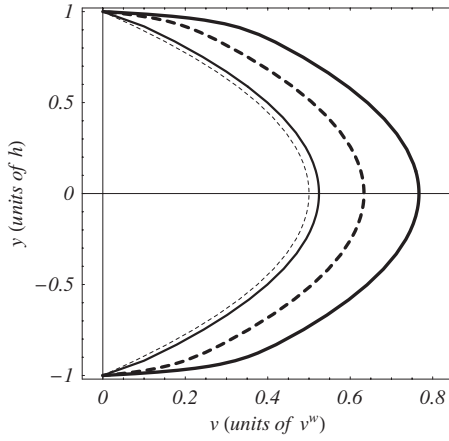


FIG. 6. The Poiseuille flow profile (59) is displayed for several values of the parameter  $c_a$ :  $c_a=0$  (thick line),  $c_a=1$  (thick dashed line),  $c_a=10$  (thin line), and  $c_a=\infty$  (thin dashed line). The remaining parameters are  $Q=8$ ,  $h/\ell=9$ .

$$v(y) = \frac{1}{2} \gamma_2 h \left( \frac{y^2}{h^2} - 1 \right) + \gamma_3 \ell [\cosh(y/\ell) - \cosh(h/\ell)]. \quad (54)$$

The coefficients  $\alpha_2, \alpha_3, \gamma_2, \gamma_3$  must be determined from the differential equations (31), (32) and the boundary condition (33) with (34). In particular, the solution of the inhomogeneous equation (32) leads to

$$\alpha_2 = -\tau_{ap} h \eta^{-1} \frac{\delta P}{L}, \quad (55)$$

the homogeneous part of this differential equation is already obeyed by the ansatz (52). The boundary condition (33) leads to

$$\alpha_2 = -\alpha_3 [\sinh(h/\ell) + c_a \cosh(h/\ell)]. \quad (56)$$

From the differential equation (39) follows

$$\alpha_2 = -\tau_{ap} \gamma_2, \quad Q \alpha_3 = \tau_{ap} \gamma_3. \quad (57)$$

Insertion of these relations into (56) yields

$$\gamma_2 = h \eta^{-1} \frac{\delta P}{L}, \quad Q \gamma_2 = \gamma_3 [\sinh(h/\ell) + c_a \cosh(h/\ell)]. \quad (58)$$

The resulting solution for the velocity field is

$$v(y) = -\eta^{-1} \frac{\delta P}{L} h^2 \left[ \frac{1}{2} \left( 1 - \frac{y^2}{h^2} \right) + Q \frac{\ell}{h} \frac{\cosh(h/\ell) - \cosh(y/\ell)}{\sinh(h/\ell) + c_a \cosh(h/\ell)} \right]. \quad (59)$$

Clearly, for  $Q > 0$  the flow is faster than for  $Q=0$ . In Fig. 6 the Poiseuille flow profile is plotted for  $Q=8$  and different values of the boundary parameter  $c_a$ . For  $c_a=0$ , we have a high slip length, where the flow is much faster than the ordinary Poiseuille flow without slip. The flow slows down for

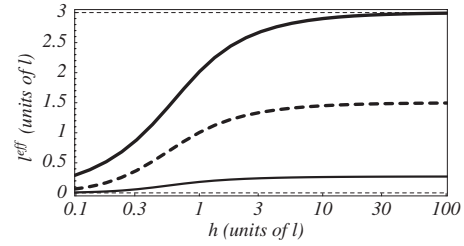


FIG. 7. The effective slip length (63) vs  $h$  is plotted. The same conditions as in Fig. 6 are considered with parameters  $Q=8$  and  $c_a=0$  (thick line),  $c_a=1$  (thick dashed line),  $c_a=10$  (thin line).

higher values of  $c_a$  and reaches the Poiseuille flow without slip in the limit  $c_a \rightarrow \infty$ .

Let  $V(Q)$  be the flow velocity in the middle, i.e., for  $y=0$  as a function of the model parameter  $Q$ . From (59) one infers for the effective slip velocity

$$\delta v^{\text{eff}} = V(Q) - V(0) = V(0) 2Q \frac{\ell}{h} \frac{\cosh(h/\ell) - 1}{\sinh(h/\ell) + c_a \cosh(h/\ell)}, \quad (60)$$

$$V(0) = -\eta^{-1} \frac{\delta P}{2L}.$$

The solution for  $\alpha$  is

$$\alpha(y) = -\tau_{ap} h \eta^{-1} \frac{\delta P}{L} \left( \frac{y}{h} - \frac{\sinh(y/\ell)}{\sinh(h/\ell) + c_a \cosh(h/\ell)} \right). \quad (61)$$

The flux  $J=J(Q)$  per unit length in the transverse direction is given by

$$J = \int_{-h}^h dy v(y) = 2 \int_0^h dy v(y) = -\frac{2}{3} h^3 \eta^{-1} \frac{\delta P}{L} \left( 1 + 3Q \frac{\ell}{h} \frac{1 - \frac{\ell}{h} \tanh(h/\ell)}{c_a + \tanh(h/\ell)} \right). \quad (62)$$

When the velocity is not coupled with the alignment ( $Q=0$ ) but when a velocity slip characterized by the slip length  $\ell_v$  is considered, the ratio of the flux with and without slip is given by  $1 + 3\ell_v/h$ . The relation (62) corresponds to such an expression, now with an effective slip length

$$\ell_v^{\text{eff}} = \ell Q \frac{1 - \frac{\ell}{h} \tanh(h/\ell)}{c_a + \tanh(h/\ell)}. \quad (63)$$

For  $\ell \ll h$ , this expression reduces to

$$\ell_v^{\text{eff}} \rightarrow \frac{\ell Q}{1 + c_a}. \quad (64)$$

In Fig. 7, the dependence of the effective slip length on  $h$  is displayed. As in previous plots the influence is most significant for  $c_a=0$  and less for higher values. The effective slip length saturates for relatively small values of the ratio

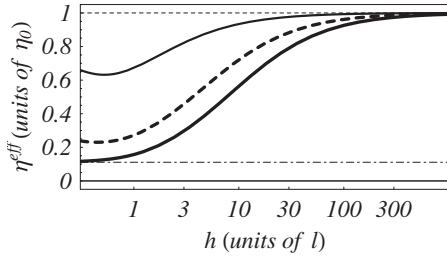


FIG. 8. The reduced effective viscosity  $\eta^{\text{eff}}/\eta$  (65) as a function of  $h/\ell$  is plotted. The parameters are  $Q=8$  and  $c_a=0$  (thick line),  $c_a=1$  (thick dashed line),  $c_a=10$  (thin line).

$h/\ell$  to a value given by Eq. (64). This implies that the ratio of  $\ell^{\text{eff}}/h$  goes to zero as in the Couette flow and for high values of  $h$  the apparent slip could be neglected.

Since  $J \sim \eta^{-1}$ , an effective viscosity for the Poiseuille flow is defined by

$$\eta_{\text{eff}} = [J(0)/J(Q)]\eta = \eta \left( 1 + 3Q \frac{\ell}{h} \frac{1 - \frac{\ell}{h} \tanh(h/\ell)}{c_a + \tanh(h/\ell)} \right)^{-1}. \quad (65)$$

In the limit  $\ell \ll h$  one has

$$\eta_{\text{eff}} \rightarrow \eta \frac{1 + c_a}{1 + c_a + 3Q \frac{\ell}{h}}. \quad (66)$$

In Fig. 8 the effective viscosity vs  $h/\ell$  is plotted. Again, for high values of  $h$  compared to  $\ell$  we arrive at a region where the apparent slip effect is not important but for smaller values of  $h/\ell$  the effective viscosity decreases. The lowest value of the effective viscosity is  $\eta^{\text{eff}} = \eta/9$ , which is attained for  $c_a=0$ . For  $c_a \neq 0$ , the effective viscosity reaches a minimum and increase after that minimum for smaller values of  $h/\ell$  again. This behavior can be observed for very small values of ratios  $h/\ell$  which are not physically relevant here and might be an artefact of the approximations employed. The reason is that in the limit  $h \rightarrow 0$  the value  $\eta^{\text{eff}}$  depends on the parameter  $c_a$ . The limit value is  $1/9$  for  $c_a=0$  whereas the limit value is  $1$  if  $c_a \neq 0$ .

### E. Flow down an inclined plane

For Newtonian fluids, the analysis of the gravity-driven flow down an inclined plane can be done in a similar manner as the case of Poiseuille flow. Here, however, different boundary conditions at the free surface lead to different flow profiles compared to the Poiseuille flow.

We choose the  $x$  and  $y$  axis parallel and perpendicular to the inclined plane, respectively, such that  $y=0$  defines the solid plane, while the free surface of the fluid film is located at  $y=h$ . The fluid film is assumed to be thin enough such that variations of the gravity force density  $\mathbf{F} = \rho g(\sin \beta, -\cos \beta, 0)$  within the fluid layer can be neglected. The angle that the inclined plane forms with the horizontal axis is denoted by  $\beta$ . An illustration is given in Fig. 9

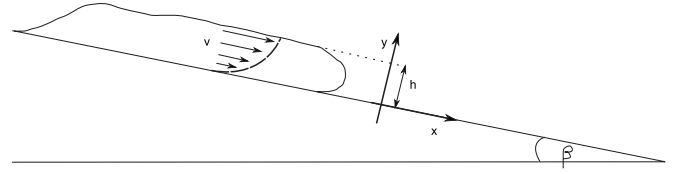


FIG. 9. Sketch of the inclined plane.

Assuming incompressibility and no mechanical slip at the bottom plane, the velocity field is again of the form  $\mathbf{v} = v(y)\mathbf{e}^x$ .

At the free surface  $y=h$ , we impose the following boundary conditions: First, the scalar pressure  $p$  must match the atmospheric pressure  $p_0$ . Second, we require that no tangential stresses exist at the free surface,  $P_{yx}|_h=0$ . Third, the boundary condition (33) for the alignment flux at the free surface  $\alpha(h) = -c_h \ell \alpha'(h)$  is different from that at the bottom plane  $\alpha(0) = c_0 \ell \alpha'(0)$  due to the different interactions the fluid experiences near the confining wall ( $c_0$ ) and near the free surface ( $c_h$ ).

From the  $y$  component of the momentum balance equation, the profile of the scalar pressure  $p(y) = p_0 + \rho g(h-y)\cos \beta$  is found to be the same as for a Newtonian liquid.

Inserting the constitutive relations (6) and (7), the second boundary condition at the free surface becomes  $-2\eta_{\text{iso}}\Gamma_{yx}|_h + \sqrt{2}p_{\text{kin}}(\tau_{ap}/\tau_a)\Phi_{yx}|_h = 0$ . We note, that the velocity gradient need not vanish at the free surface due to the alignment contribution to the pressure tensor.

In the present case, the stationary solution to (21) reduces not to (31) but  $\alpha - \ell \alpha' = G(h-y)$ , with  $G = \rho g \tau_{ap} \sin \beta / \eta$ . The general solution to this equation reads  $\alpha(y) = \alpha_1 e^{y/\ell} + \alpha_2 e^{-y/\ell} + G(y-h)$ . The boundary conditions lead to the final expressions

$$\alpha(y) = \frac{G\ell}{Z} \left[ -c_h \sinh(y/\ell) - c_0 c_h \cosh(y/\ell) - \left( c_0 + \frac{h}{\ell} \right) \sinh[(y-h)/\ell] + c_h \left( c_0 + \frac{h}{\ell} \right) \cosh[(y-h)/\ell] \right] + G(y-h) \quad (67)$$

with  $Z = (1 + c_0 c_h) \sinh(h/\ell) + (c_0 + c_h) \cosh(h/\ell)$ .

The resulting solution for the velocity field is

$$v(y) = v_0 \left[ \frac{1}{2} \left( 2 - \frac{y}{h} \right) \frac{y}{h} + Q \left( \frac{\ell}{h} \right)^2 \frac{1}{Z} F(y/\ell) \right], \quad (68)$$

where  $v_0 = \rho g h^2 \sin \beta / \eta$  is 2 times the velocity at the free surface for Newtonian fluids,  $v(y=h, Q=0) = v_0/2$ . The modification of the flow profile due to the alignment is described by

$$F(y/\ell) = c_h [1 - \cosh(y/\ell)] - c_0 c_h \sinh(y/\ell) + \left( c_0 + \frac{h}{\ell} \right) \{ \cosh(h/\ell) - \cosh[(y-h)/\ell] \} + c_h \left( c_0 + \frac{h}{\ell} \right) \{ \sinh(h/\ell) + \sinh[(y-h)/\ell] \}. \quad (69)$$

The flux  $J(Q)$  down the inclined plane per unit length in the transverse direction is found to be given by

$$J(Q) = \int_0^h dy v(y) = \frac{1}{3} v_0 h \left( 1 + \frac{3Q\ell}{Z h} [k_1 \sinh(h/\ell) + k_2 \cosh(h/\ell)] \right) \quad (70)$$

with  $k_1 = c_h(1 + c_0\ell/h) - (\ell/h)k_2$ ,  $k_2 = 1 + (c_0 + c_h)\ell/h$ . From the flux  $J$ , the apparent slip velocity is defined by [36]

$$\delta v^{\text{eff}} = \left. \frac{\partial(J/h^2)}{\partial(1/h)} \right|_{\rho g h \sin \beta}, \quad (71)$$

where the derivative is taken at constant surface shear stress (in absence of coupling). From Eq. (70) one finds

$$\delta v^{\text{eff}} = v_0 \frac{Q}{Z} [k_1 k_2 + (c_h^2 + k_2^2)(\ell/h)^2 \cosh(h/\ell) \sinh(h/\ell)]. \quad (72)$$

A particularly interesting case is a vanishing alignment flux at the bottom plane and vanishing alignment flux gradient at the surface. In this case, the boundary conditions become  $\alpha(0)=0$ ,  $\alpha'(h)=0$ , then one has

$$v^{\infty}(y) = \frac{\rho g \sin \beta}{\eta} h^2 \left[ \frac{1}{2} \left( 2 - \frac{y}{h} \right) \frac{y}{h} + Q \frac{\ell^2}{h^2} \left( \frac{h}{\ell} \sinh(y/\ell) - \cosh(y/\ell) + 1 \right) \right]. \quad (73)$$

Note, that the special case (73) can be derived from Eq. (68) for  $c_0=0$ ,  $c_h \rightarrow \infty$  only in the limiting case  $h/\ell \ll 1$ . In this case, the apparent velocity slip (72) simplifies to

$$\delta v^{\infty, \text{eff}} = v_0 Q \left( \frac{\ell}{h} \right)^2 \left[ \left( 2 - \frac{\ell}{h} \right) \cosh(h/\ell) + \left( 1 - 3 \frac{\ell}{h} \right) \sinh(h/\ell) \right]. \quad (74)$$

In this approximation the flow profile is very similar to the plane Poiseuille flow cut in the middle plane and for  $h/\ell < 0.1$  it cannot be distinguished in graphical diagrams. In the limiting case  $h/\ell \gg 1$ ,  $c_0=0$  and  $c_h \rightarrow \infty$  the influence of boundary conditions become smaller and for  $h/\ell > 1000$  the flow profile coincides with the plane Poiseuille flow cut in the middle for graphical accuracy. In Fig. 10 the flow profile for the flow down an inclined plane is compared with Poiseuille flow cut in the middle (dashed line) between the limiting cases for  $c_0=0$  and  $c_h \rightarrow \infty$ . In these regimes the difference between the Poiseuille flow and the inclined flow profile is significant and becomes smaller for higher values of the ratio  $h/\ell$ .

### F. Alignment

For the special cases considered in this section, viz., isotropic phase and small shear rates, only the  $xy$  component of the alignment tensor is affected by the flow. The alignment tensor is written as, cf. (30),

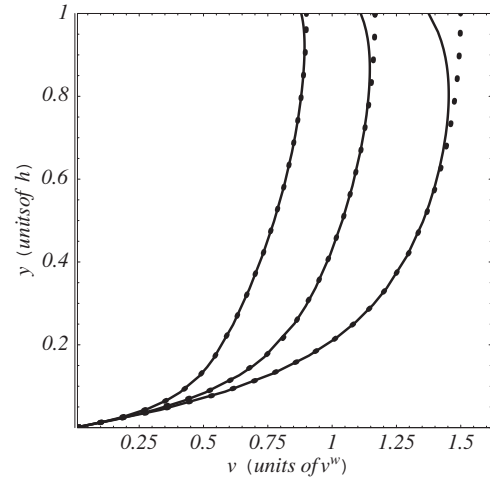


FIG. 10. The flow profile of the flow down an inclined plane is displayed for several values of the parameter  $h/\ell=8, 12, 20$  (from the right to the left). The remaining parameters are  $c_0=c_a=0$ ,  $c_h=\infty$ ,  $Q=8$ . The dashed line shows one-half of the Poiseuille flow profile for the same parameter.

$$a_{\mu\nu} = \sqrt{2} a(y) e_{\nu}^x e_{\mu}^y + \dots \quad (75)$$

The ellipses stand for the other components which could be nonzero, due the influence of the walls. In the isotropic phase, relation (12) is equivalent to

$$a - \xi^2 a'' = A^{-1} \alpha, \quad \xi^2 = A^{-1} \xi_0^2, \quad (76)$$

where the elastic coherence length  $\xi$  is used. For  $\xi=0$  the alignment  $a(y)$  is determined by the quantity  $\alpha(y)$  as computed above. For  $\xi \neq 0$ , on the other hand, the value of  $a$ , i.e., of the  $xy$  component of the alignment tensor can and must be prescribed in order to obtain a unique solution for the alignment. It is recalled that the boundary condition given above was not formulated directly for the alignment tensor but rather for the derivative of the potential function with respect to the alignment.

As before, the plane Couette flow and plane Poiseuille flow geometries are treated. In analogy to (35) the ansatz

$$a(y) = a_0 + a_1 \cosh(y/\ell) + b \cosh(y/\xi), \quad \xi \neq \ell, \quad (77)$$

or

$$a(y) = a_0 + a_1 (y/\ell) \sinh(y/\ell) + b \cosh(y/\ell), \quad \xi = \ell \quad (78)$$

is made for the Couette case. Again it is assumed that the walls at  $y=h$  and at  $y=-h$  are identical. The coefficients  $a_0, a_1$  follow from the differential equation (76), the coefficient  $b$  is fixed by the value  $a^w$  of the alignment at the wall. More specifically, one obtains

$$a_0 = A^{-1} \alpha_0, \quad a_1 = [1 - (\xi^2/\ell^2)]^{-1} A^{-1} \alpha_1, \quad \xi \neq \ell, \quad (79)$$

and

$$a_0 = A^{-1} \alpha_0, \quad a_1 = -\frac{1}{2} A^{-1} \alpha_1, \quad \xi = \ell, \quad (80)$$

Similarly, for the Poiseuille flow between identical walls we use, cf. (52),

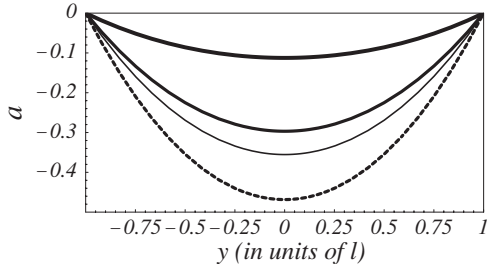


FIG. 11. The  $xy$  component of the alignment tensor is plotted for plane Couette flow for several values of the parameter  $c_a$ . The parameters are chosen as  $Q=8$ ,  $A=1$ ,  $\xi=0.3$ ,  $l=0.2$ ,  $\tau_{ap}=0.5$ ,  $v^w=1$ ,  $h/l=1$ ,  $a(h)=0$  and  $c_a=0$  (thick line),  $c_a=10$  (middle thick line),  $c_a=20$  (thin line),  $c_a=\infty$  (dashed line).

$$a(y) = a_2(y/\ell) + a_3 \sinh(y/\ell) + b_1 \sinh(y/\xi) + b_2 \cosh(y/\xi), \quad \xi \neq \ell, \quad (81)$$

or

$$a(y) = a_2(y/\ell) + a_3(y/\ell)\cosh(y/\ell) + b_1 \sinh(y/\xi) + b_2 \cosh(y/\xi), \quad \xi = \ell. \quad (82)$$

The differential equation (76) yields relations for the coefficients  $a_2, a_3$  which are identical to (79) and (80) with the subscripts 0, 1 replaced by 2, 3. The coefficients  $b_1, b_2$  are determined by the alignment at the wall. In Figs. 11 and 12 the  $xy$  component of the alignment tensor for the Couette flow and the Poiseuille flow is displayed, respectively. At the boundary we used uniaxial alignment  $\mathbf{a} = \sqrt{3/2} a_{eq} \mathbf{n} \mathbf{n}$ . In our case the director  $\mathbf{n}$  lies perpendicular to the  $xy$  plane. The  $xy$  component of the alignment tensor is then  $a=0$ . Figures 11 and 12 show a significant effect on the flow alignment by the apparent slip parameter  $c_a$ . In the Couette flow the shape of the curve is only mildly affected whereas the minima grows. This means for small values of  $c_a$  that the flow alignment angle of the molecules in the middle of the Couette cell deviates less from the flow alignment angle of the molecules at the wall. In the Poiseuille case, the alignment solutions are antisymmetric with respect to the middle plane as a consequence of the symmetry of the velocity profile. As in the Couette flow, curves for several parameter values  $c_a$  are between the limiting curves for  $c_a \rightarrow \infty$  indicated by the dashed

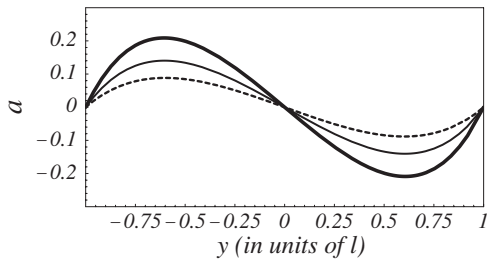


FIG. 12. The  $xy$  component of the alignment tensor is plotted for plane Poiseuille flow for several values of the parameter  $c_a$ . The parameters are  $Q=8$ ,  $A=1$ ,  $\xi=0.1$ ,  $l=0.2$ ,  $\tau_{ap}=0.5$ ,  $v^w=1$ ,  $h=1$ ,  $a(h)=0$  and  $c_a=0$  (thick line),  $c_a=1$  (middle thick line),  $c_a=\infty$  (dashed line).

line and for  $c_a=0$  (thick line). High values of the parameter  $c_a$  lead to small flow alignment angle in the bulk except for  $y=0$  where all curves are intersecting.

### G. Couette flow in cylindrical geometry

In order to determine material functions of non-Newtonian fluids, it is common practice to carry out shear experiments in different geometries (cone-plate or cylindrical geometry). Here we consider a fluid between two coaxial cylinders which are in relative rotation. The inner-cylinder radius is denoted by  $r_i > 0$  and the outer cylinder by  $r_o$  ( $r_o > r_i$ ). We assume that the cylinders are infinite in extent to avoid boundary effects from the top and the bottom of the cylinder. According to the special symmetry we choose polar coordinates, the appropriate velocity field is taken as

$$\mathbf{v} = [0, u(r), 0]^T \quad (83)$$

and the orthonormal tensor basis

$$\begin{aligned} \mathbf{T}^0 &= \sqrt{3/2} \mathbf{e}_z \mathbf{e}_z, & \mathbf{T}^1 &= 1/\sqrt{2} (\mathbf{e}_r \mathbf{e}_r - \mathbf{e}_\phi \mathbf{e}_\phi) \\ \mathbf{T}^2 &= \sqrt{2} \mathbf{e}_r \mathbf{e}_\phi, & \mathbf{T}^3 &= \sqrt{2} \mathbf{e}_r \mathbf{e}_z, & \mathbf{T}^4 &= \sqrt{2} \mathbf{e}_\phi \mathbf{e}_z, \end{aligned} \quad (84)$$

which is similar to the Cartesian orthonormal tensor basis used in [37]. Analog to the preceding section we choose a special Ansatz for the strain tensor  $\mathbf{\Gamma}$  and  $\mathbf{\Phi}$ ,

$$\mathbf{\Gamma} = \frac{1}{\sqrt{2}} \gamma(r) \mathbf{T}^2, \quad (85)$$

$$\mathbf{\Phi} = \alpha(r) \mathbf{T}^2. \quad (86)$$

With the help of this Ansatz, Eqs. (19) and (21) can be rewritten as

$$\alpha(r) \mathbf{T}^2 - \ell_a^2 \mathbf{T}^2 \Delta_{r,\phi} \alpha(r) - \ell_a^2 \alpha(r) \Delta_{r,\phi} \mathbf{T}^2 = -\sqrt{2} \tau_{ap} \gamma(r) \mathbf{T}^2, \quad (87)$$

$$p_{\text{kin}} \sqrt{2} \frac{\tau_{ap}}{\tau_a} \nabla_{r,\phi} \alpha(r) \cdot \mathbf{T}^2 + p_{\text{kin}} \sqrt{2} \frac{\tau_{ap}}{\tau_a} \alpha(r) \nabla_{r,\phi} \cdot \mathbf{T}^2 = \eta_{\text{iso}} \Delta_{r,\phi} \mathbf{v}, \quad (88)$$

where  $\Delta_{r,\phi}$  and  $\nabla_{r,\phi}$  are the Laplacian and the gradient in polar coordinates, respectively. Equation (88) can be rearranged as

$$\nabla_{r,\phi} \cdot \left( \eta_{\text{iso}} \mathbf{\Gamma} - 1/\sqrt{2} \frac{\tau_{ap}}{\tau_a} p_{\text{kin}} \alpha(r) \mathbf{T}^2 \right) = 0, \quad (89)$$

when the incompressibility condition is used. The solution of Eq. (89) is given by

$$\gamma(r) = \frac{1}{\eta_{\text{iso}}} \frac{\tau_{ap}}{\tau_a} p_{\text{kin}} \alpha(r) + c/r^2 \quad (90)$$

and leads with Eq. (87) to a Bessel differential equation for the function  $\alpha$ ,

$$\alpha(r) - \ell \Delta_{r,\phi} \alpha(r) = c/r^2 \quad (91)$$

or explicitly

$$r^2\alpha''(r) + r\alpha'(r) - \left(1 + \frac{r^2}{\ell^2}\right)\alpha(r) = f(r). \quad (92)$$

In our case  $f(r) = c/r^2$ . The homogeneous solutions are modified Bessel functions (Bessel functions with pure imaginary argument) which are denoted as  $\mathfrak{J}_\lambda$  (first kind of order  $\lambda$ ) and  $\mathfrak{K}_\lambda$  (second kind of order  $\lambda$ ). The particular solution of the Bessel equation can be derived by

$$\alpha^p(r) = \frac{\pi}{2}\mathfrak{K}_\lambda(r) \int r\mathfrak{J}_\lambda(r)f(r)dr - \frac{\pi}{2}\mathfrak{J}_\lambda(r) \int r\mathfrak{K}_\lambda(r)f(r)dr, \quad (93)$$

such that the general solution can be written as

$$\alpha(r) = \alpha_1\mathfrak{J}_1(\hat{r}) + \alpha_1\mathfrak{K}_1(\hat{r}) + \frac{\pi}{2}c\ell^2 \left( \mathfrak{K}_1(\hat{r}) \int \mathfrak{J}_1(\hat{r})/\hat{r}d\hat{r} - \mathfrak{J}_1(\hat{r}) \int \mathfrak{K}_1(\hat{r})/\hat{r}d\hat{r} \right). \quad (94)$$

Here we use the abbreviation  $\hat{r} = r/\ell$ . The solution of the integrals are generalized hypergeometric functions and Majer  $G$  functions. In principle, it is possible to use the exact solution of  $\alpha$  for further calculations. In many applications, however, cylindrical Couette flow is considered with large radii of  $r_i$  and  $r_o$ , i.e.,  $r_i, r_o \gg 1$ . In that case, the modified Bessel functions can be approximated by  $\mathfrak{J}_\lambda(r) \sim \frac{1}{\sqrt{r}}e^r$  and  $\mathfrak{K}_\lambda(r) \sim \frac{1}{\sqrt{r}}e^{-r}$  [38,39], so that the integration is trivial and the general solution for not too small values of  $r_i, r_o$  is

$$\alpha(r) = \frac{1}{\sqrt{\hat{r}}}(\alpha_1 e^{\hat{r}} + \alpha_2 e^{-\hat{r}}) + \alpha_0. \quad (95)$$

The integration constant was denoted by  $\alpha_0$ . The coefficients  $\alpha_1$  and  $\alpha_2$  are determined by the boundary conditions for the alignment flow  $\Phi$ ,

$$\alpha(r_i) = c_a\ell\alpha'(r_i), \quad \alpha(r_o) = -c_a\ell\alpha'(r_o). \quad (96)$$

The shear rate  $\gamma(r)$  according to Eq. (90) is given by

$$\gamma(r) = -Q\frac{1}{\sqrt{\hat{r}}}(\alpha_1 e^{\hat{r}} + \alpha_2 e^{-\hat{r}}) + \gamma_1/r^2 + \gamma_0 \quad (97)$$

and the velocity profile can be derived by integration as

$$v(r) = -Q\sqrt{\pi\ell}[\alpha_1(c_a\ell, r_i, r_o)\text{erfi}[\sqrt{\hat{r}}] + \alpha_2(c_a\ell, r_i, r_o)\text{erf}[\sqrt{\hat{r}}]] + \gamma_0 r - \gamma_1/r, \quad (98)$$

where  $\text{erf}[x]$  denotes the error function and  $\text{erfi}[z] = -i\text{erf}[iz]$ . The coefficients  $\gamma_0$  and  $\gamma_1$  are determined by the no-slip conditions of the velocity at the boundary  $r_i$  and  $r_o$ .

For a better comparison to the plane Couette flow considered above, we introduce new coordinates. We denote the variables  $r_o - r_i = 2h$ ,  $\xi = \{r | r \in [r_i, r_o]\}$  and  $r_m = r_i + (r_o - r_i)/2$ . The boundary conditions (96) reduce to

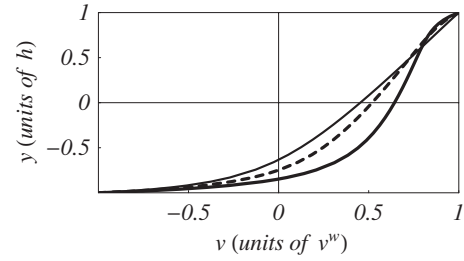


FIG. 13. The velocity vs the distance in units of  $h$  is plotted for Couette flow in cylindrical geometry. The chosen model parameters are  $Q=8$ ,  $h/\ell=9$ ,  $r_m/\ell=10$ , and  $c_a=0$  (thick line),  $c_a=3$  (thick dashed line),  $c_a=100$  (thin line).

$$\alpha(r_m, -h) = c_a\ell\alpha'(r_m, -h), \quad \alpha(r_m, h) = -c_a\ell\alpha'(r_m, h). \quad (99)$$

We assume for the velocity boundary conditions  $v(r_i=r_m-h) = v(r_m, -h) = -v^w$  and  $v(r_o=r_m+h) = v(r_m, h) = v^w$  that is the outer cylinder is moved by  $v^w$  and the inner by  $-v^w$ . In these coordinates the velocity profile is a function of  $\xi$  and with the parameters  $c_a, \ell, h, r_m, v^w$ ,

$$v(\xi; c_a, \ell, h, r_m, v^w) = -Q\sqrt{\pi\ell}[\alpha_1(c_a, \ell, r_i, r_o)\text{erfi}[\sqrt{\hat{\xi} + \hat{r}_m}] + \alpha_2(c_a, \ell, r_i, r_o)\text{erf}[\sqrt{\hat{\xi} + \hat{r}_m}]] + \gamma_0(r_m + \xi) - \gamma_1/(r_m + \xi). \quad (100)$$

We analytically calculated the coefficients  $\alpha_1$ ,  $\alpha_2$ ,  $\gamma_0$ , and  $\gamma_1$  with the computer algebra program MATHEMATICA4.1. In Fig. 13, the velocity profile is plotted for  $Q=8$ ,  $h/\ell=9$ ,  $l=1$ , and  $r_m/\ell=10$ . The velocity is presented in units of the wall velocity  $v^w$  and  $y$  denotes  $\xi/\ell$ . The thick curve pertains to the highest possible boundary effect ( $c_a=0$ ) for  $Q=8$  fixed. For high values of the coupling of the alignment to the pressure tensor the apparent slip becomes stronger as Fig. 14 shows. As in the plane Couette flow, the extrapolation of the velocity in the center towards the wall is smaller than the wall velocity  $v^w$  and for  $c_a \rightarrow \infty$  the flow profile reaches the cylindrical Couette flow without apparent slip. In contradistinction to the plane Couette flow, the velocity profile in cylindrical geometry is asymmetric. That is a direct consequence of the radial geometry, i.e., of the term  $1/(r_m + \xi)$ . In the case where  $r_m \gg h$  we can approximate  $1/(r_m + \xi) \approx 1/r_m$  so that

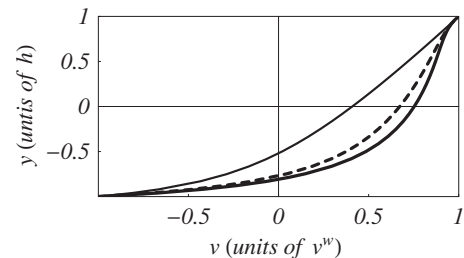


FIG. 14. Same as Fig. 12 but for parameters  $r_m/\ell=11$ ,  $h/\ell=9$ ,  $c_a=0$ , and  $Q=10$  (thick line),  $Q=1$  (thick dashed line),  $Q=0$  (thin line).

our results for the cylindrical Couette flow can be compared to the results of plane Couette flow directly.

In particular, the velocity profile cannot be distinguished from the plane Couette flow profile in Fig. 2 if the same parameter values are used.

## V. CONCLUDING REMARKS

In microfluidics, the flow behavior can be strongly affected by boundary conditions. In this paper we show that boundary conditions derived in the framework of nonequilibrium thermodynamics for molecular liquids lead to an apparent slip in the different flow geometries. In a plane Couette flow as well as in a cylindrical Couette flow, the velocity in the bulk extrapolated towards the wall is slower than the wall velocity. The cylindrical Couette flow is influenced by the radial geometry leading to the nonsymmetrical flow profile, but qualitatively the effect of the alignment flow at the boundary gives the same apparent slip and coincides in the limit for large radii with the plane Couette flow profile. On the other hand, for Poiseuille flow and the flow down an inclined plane, the flow in the bulk becomes faster caused by boundary effects. We have shown for the case of a plane Couette flow and a plane Poiseuille flow, that as a consequence of the alignment flow boundary conditions, the effective viscosity decreases if the length scale ( $h$ ) of the device is comparable with the slip length. This also applies to the other geometries.

In all cases the boundary effects are dramatic for values of  $h$  comparable with the length  $\ell$ . On the other hand, if the systems length is much larger than  $\ell$ , all these boundary effects are negligible, as expected.

The microscopic interpretation of the boundary conditions is a challenging problem in particular for complex fluids. The strong slip limit  $h \ll \ell$  of the expressions given in this paper should be taken with caution. Based on experience with rarefied gas dynamics, strong deviations from hydrodynamics require modified differential equations and additional boundary conditions which are not considered here. For simple fluids, a lower bound on  $h/\ell$  for a hydrodynamic description has been inferred from molecular dynamics simulations in [40].

So far, specific applications were restricted to the isotropic phase and linear flow regime. The nonlinear flow behavior in the isotropic and nematic phase can be studied by numerical solutions. This is also possible for tumbling nematics as considered in [25,34]. Preliminary results are available.

## ACKNOWLEDGMENTS

This research has been performed under the auspices of the Sonderforschungsbereich 448 Mesoskopisch strukturierte Verbundsysteme financially supported by the Deutsche Forschungsgemeinschaft (DFG). This project has been supported in part through EU-NSF Contract No. NMP3-CT-2005-016375 of the European Community.

- 
- [1] F. R. W. McCourt, J. J. M. Beenakker, W. E. Köhler and I. Kuscer, *Nonequilibrium Phenomena in Polyatomic Gases* (Clarendon, Oxford, 1990), Vols. 1 and 2.
  - [2] T. M. Squires and S. R. Quake, *Rev. Mod. Phys.* **77**, 977 (2005).
  - [3] N. V. Priezjev and S. M. Troian, *Phys. Rev. Lett.* **92**, 018302 (2004).
  - [4] C. Neto, D. R. Evans, E. Bonaccorso, H.-J. Butt, and V. S. J. Craig, *Rep. Prog. Phys.* **68**, 2859 (2005).
  - [5] E. Lauga, M. P. Brenner, and H. A. Stone, in *Handbook of Experimental Fluid Dynamics*, edited by J. Foss, C. Tropea, and A. Yarin (Springer, New York, 2005).
  - [6] C. Cottine-Bizonne *et al.*, *Nat. Mater.* **2**, 238 (2003).
  - [7] P. Joseph and P. Tabeling, *Phys. Rev. E* **71**, 035303(R) (2005).
  - [8] D. C. Trethewey and C. D. Mainhart, *Phys. Fluids* **14**, L9 (2002).
  - [9] R. Benzi, L. Biferale, M. Sbragaglia, S. Succi, and F. Toschi, *Math. Comput. Simul.* **72**, 84 (2006).
  - [10] S. P. Meeker, R. T. Bonnecaze, and M. Cloitre, *Phys. Rev. Lett.* **92**, 198302 (2004).
  - [11] V. S. J. Craig, C. Neto, and D. R. M. Williams, *Phys. Rev. Lett.* **87**, 054504 (2001).
  - [12] C. Pastorino, K. Binder, T. Kreer, and M. Müller, *J. Chem. Phys.* **124**, 064902 (2006).
  - [13] L. Waldmann, *Z. Naturforsch. A* **22a**, 1269 (1967).
  - [14] H. Vestner, *Z. Naturforsch. A* **28a**, 869 (1973).
  - [15] S. Hess and H.-M. Koo, *J. Non-Equilib. Thermodyn.* **14**, 159 (1989).
  - [16] R. Fetzer, M. Rauscher, A. Münch, B. A. Wagner, and K. Jacobs, *Europhys. Lett.* **75**, 638 (2006).
  - [17] D. Bedeaux, A. M. Albano, and P. Mazur, *Physica A* **82**, 438 (1976).
  - [18] A. M. Albano and D. Bedeaux, *Physica A* **147**, 407 (1987).
  - [19] H. C. Öttinger, *Phys. Rev. E* **73**, 036126 (2006).
  - [20] G. G. Fuller, *Optical Rheometry of Complex Fluids* (Oxford University Press, New York, 1995).
  - [21] S. Hess, *Z. Naturforsch. A* **30a**, 728 (1975).
  - [22] C. Pereira Borgmeyer and S. Hess, *J. Non-Equilib. Thermodyn.* **20**, 359 (1995).
  - [23] S. Hess and I. Pardowitz, *Z. Naturforsch. A* **36a**, 554 (1981).
  - [24] G. Marrucci and F. Greco, *Mol. Cryst. Liq. Cryst.* **206**, 17 (1991); M. Kröger and H. S. Sellers, in *Complex Fluids*, edited by L. Garrido, *Lecture Notes in Physics* 415 (Springer, New York, 1992), pp. 295–301; G. Sgalari, G. L. Leal, and J. J. Feng, *J. Non-Newtonian Fluid Mech.* **102**, 361 (2002).
  - [25] G. Rienäcker, M. Kröger, and S. Hess, *Phys. Rev. E* **66**, 040702(R) (2002); *Physica A* **315**, 537 (2002).
  - [26] B. K. Gupta, S. Hess, and A. D. May, *Can. J. Phys.* **50**, 778 (1972).
  - [27] S. Hess, *Z. Naturforsch. A* **28a**, 861 (1973).
  - [28] G. Rienäcker and S. Hess, *Physica A* **267**, 294 (1999).
  - [29] S. Hess, *J. Non-Equilib. Thermodyn.* **11**, 176 (1986).

- [30] S. Hess, *Z. Naturforsch. A* **31a**, 1034 (1976).
- [31] S. Hess, in *Electro-Optics and Dielectrics of Macromolecules and Colloids*, edited by B. R. Jennings, (Plenum, New York 1979).
- [32] M. Doi, *Ferroelectrics* **30**, 247 (1980); *J. Polym. Sci., Polym. Phys. Ed.* **19**, 229 (1981).
- [33] C. Schneggenburger, M. Kröger, and S. Hess, *J. Non-Newtonian Fluid Mech.* **62**, 235 (1996).
- [34] S. Heidenreich, P. Ilg, and S. Hess, *Phys. Rev. E* **73**, 061710 (2006).
- [35] L. Waldmann and H. Vestner, *Physica A* **99**, 1 (1979).
- [36] Y. Cohen, in *Encyclopedia of fluid mechanics*, edited by N. P. Cheremisinoff, Vol. 7 (Gulf, Houston, 1986).
- [37] P. Kaiser, W. Wiese, and S. Hess, *J. Non-Equilib. Thermodyn.* **17**, 153 (1992).
- [38] W. Rehwald, *Elementare Einführung in die Bessel-, Neumann- und Hankel-Funktionen*, edited by O. Zinke, and S. Hirzel (Verlag, Stuttgart, 1959).
- [39] P. Kasperkovitz, *J. Math. Phys.* **21**, 6 (1980).
- [40] L. Bocquet and J.-L. Barrat, *J. Phys.: Condens. Matter* **8**, 9297 (1996).